Magnetic Resonance in Medicine 50:839–843 (2003)

Single-Shot Magnetic Field Mapping Embedded in Echo-Planar Time-Course Imaging

Vinai Roopchansingh,* Robert W. Cox, Andrzej Jesmanowicz, B. Douglas Ward, and James S. Hyde

A technique for acquiring magnetic field maps simultaneously with gradient-recalled echo-planar time-course data is described. This technique uses a trajectory in which the central part of *k*-space is collected twice. For a 64 × 64 image acquired with a 125-kHz bandwidth, a field map suitable for geometric correction can be collected simultaneously with the echo-planar time-course data in <70 ms. The field maps generated by this technique are registered with the magnitude images because they are calculated using the same data. They do not suffer from errors due to subject motion, or from different geometric distortions that can result from using different pulse sequences. In addition to correcting geometric distortions that resulted from dynamic magnetic field perturbations, this method was used to measure field shifts arising from respiration and jaw motion across five subjects. Values ranged from 0.035 to 0.165 parts per million (ppm). Magn Reson Med 50: 839–843, 2003. © 2003 Wiley-Liss, Inc.

Key words: magnetic field mapping; real time; geometric correction; respiration artifacts; echo-planar

A high degree of magnetic field uniformity is essential for generating and collecting high-quality MRI and spectroscopy data. Echo-planar imaging (EPI) and spiral imaging require magnetic fields with perturbations of <1 part per million (ppm) because the long readout times in these techniques make them more sensitive to magnetic field inhomogeneities.

With the use of active and passive shimming techniques (1–3), it is possible to improve magnetic field homogeneity over an entire human head so that perturbations are <1 ppm everywhere except at the base of the frontal lobe and the inferior temporal lobes. However, even residual magnetic field perturbations below 1 ppm can cause geometric distortions in images.

To correct geometric distortions, information in magnetic field maps is used to shift pixels to their correct positions. The theory behind this technique and a method for implementing it were described by Jezzard and Balaban (4). However, field maps and magnitude images have generally been acquired using different pulse sequences that are subject to different geometric distortions. In addition, misregistration can be a problem if the maps and images are acquired at different times and subject motion occurs.

A technique was previously proposed (5) that enables field map data to be collected at the same time as image data. In the present work we describe that method in more detail. With this technique, magnetic field maps and magnitude images are generated in the same manner with the same data; hence there are no alignment errors. Modified echo-planar trajectories that traverse the central region of *k*-space twice (Fig. 1) are used.

These modified *k*-space trajectories permit more rapid acquisition of field maps compared to two-shot/dual-echo techniques (e.g., Ref. 6), and can be accomplished with a single RF excitation. The fraction of *k*-space that is acquired twice is proportional to the desired magnetic field map resolution in the phase-encoding direction, and nearly proportional to the time penalty incurred to acquire the extra data. Acquiring only the central fraction of *k*-space limits the accuracy of the magnetic field measurements to low spatial frequencies, but allows collection of a magnetic field map for geometric correction of image distortions on a per-shot basis. Nayak and Nishimura (7) demonstrated that magnetic field maps reconstructed from low-frequency partial *k*-space data can be used to correct the effects of magnetic field inhomogeneities in a multishot spiral technique.

A further advantage of the embedded method described here is that rapid collection of magnetic field data enables dynamic magnetic field changes due to physiological processes, such as respiration, to be monitored. Throughout the respiratory cycle, the volume of air in the lungs and the position of the chest wall and the internal organs in the thoracic cavity vary. Raj et al. (8) modeled the effect of volume changes in the lung, as well as the effect of variations in pO_2, and predicted signal intensity changes in the brain on the order of a few percent arising from this source. Other groups have utilized different approaches to measure the field changes associated with respiration (9,10) and speaking (11).

THEORY

Magnetic field maps can be computed from the phase difference between a pair of images acquired at different echo times (TEs). According to the Bloch equations,

$$S(\mathrm{TE}) = \int_z \int_y \int_x M_\perp(x, y, z, 0) \times \exp\left[-i\gamma \int_0^{\tau=\mathrm{TE}} B_z(x, y, z, \tau) d\tau \right] dx\, dy\, dz, \quad [1]$$

Department of Biophysics, Medical College of Wisconsin, Milwaukee, Wisconsin.

Grant sponsor: National Institutes of Health; Grant number: EB002014; EB00215.

R.W. Cox is now at the National Institute of Mental Health, Department of Health and Human Services, Bethesda, Maryland.

*Correspondence to: Vinai Roopchansingh, Department of Biophysics, Medical College of Wisconsin, 8701 Watertown Plank Rd., Milwaukee, WI 53226-0509. E-mail: vroopcha@mcw.edu

Received 13 December 2002; revised 23 June 2003; accepted 30 June 2003.

DOI 10.1002/mrm.10587

Published online in Wiley InterScience (www.interscience.wiley.com).

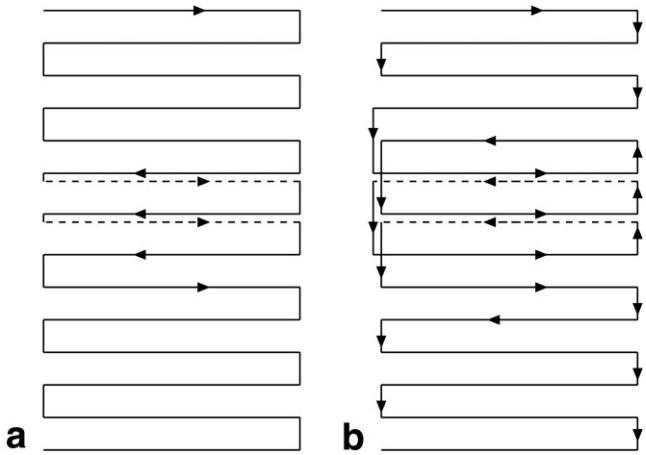

FIG. 1. Trajectories for acquiring the center of *k*-space twice: (**a**) navigator, and (**b**) moving racetrack (MRTT). Dashed lines represent repeated acquisition of a line of *k*-space.

the term in the exponent determines the phase of the detected MR signal. Acquiring the signal at different values of TE gives a phase difference that is linearly proportional to the magnetic field, $B_z(x, y, z, \tau)$.

$$\Delta\phi = \gamma\int_0^{TE+\Delta TE} B_z(x, y, z, \tau)d\tau - \gamma\int_0^{TE} B_z(x, y\, z, \tau)d\tau \approx \gamma B_z(x, y, z)\Delta TE \quad [2]$$

To the best of our knowledge, all previous field mapping methods based on this principle use separate RF pulses to generate the images at each TE. Examples of such techniques are found in Weisskoff and Davis (6) and Prammer et al. (12).

The technique presented here uses a single RF excitation in conjunction with a modified gradient-recalled echo-planar *k*-space trajectory to collect phase information at two time points. This is accomplished by changing the amplitude and sign of the phase-encoding gradients near the center of *k*-space. Two possible *k*-space trajectories have been considered. Both trajectories were designed so that pairs of corresponding *k*-space lines are acquired with a constant ΔTE. In the first trajectory, alternating phase-encode gradients for lines near the center of *k*-space can be removed (Fig. 1a), allowing the same line to be reacquired < 1 ms later. This trajectory is called "navigator-like" because of its similarity to navigator-echo techniques in which the same *k*-space information is acquired multiple times with no additional phase encoding. In the second trajectory, phase-encode gradients can be doubled in amplitude (while maintaining the same duration), and then reversed in sign to give the "moving-racetrack" trajectory (MRTT) shown in Fig. 1b. In this study we utilized the MRTT method. These trajectories are extensions of the idea originally described by Jesmanowicz (13) and recently explored by Durand et al. (14), in which the center line of *k*-space is collected twice to help correct magnetic field fluctuations and reduce *N*/2 Nyquist ghosting. The TE for the MRTT method was defined as the time when the center of *k*-space was first acquired.

MATERIALS AND METHODS

All experiments were performed on a Bruker Biospec 30/60 3 Tesla MR scanner using a local gradient coil (15) and an end-capped birdcage RF coil (inner diameter = 23 cm) with 16 elements. Experiments on human subjects were conducted in accordance with the guidelines set by the Medical College of Wisconsin Institutional Review Board.

Geometric Corrections

The field maps generated by the MRTT sequence were used to perform corrections on images containing geometric distortions. A cylindrical phantom, 165 mm in diameter, containing an internal grid and filled with a solution of 0.005 M $CuSO_4$ and 0.0938 M NaCl, was scanned using the MRTT trajectory with the following parameters: TR = 2000 ms, TE = 38.5 ms, acquisition bandwidth = 125 kHz, image matrix = 64 × 64, and 16 lines collected twice. A single human subject was scanned with the same parameters. For the phantom scans, the shim component parallel to the readout axis in the image was purposely altered so that the reliability of this method to correct for field-induced geometric distortions could be checked. For the human subject, the corrected and uncorrected data were compared to gradient-echo spin warp data to determine how well the corrected MRTT images matched the anatomical images. In addition to the *k*-space trajectory shown in Fig. 1b, the center line of *k*-space was acquired two more times after this trajectory was completed. These data were used to correct mismatches that might have occurred between corresponding echo-planar *k*-space lines acquired in positive and negative readout directions.

The algorithm used to correct geometric distortions was similar to that described by Jezzard and Balaban (4). First, magnitude images were computed from the MRTT data. For twice-acquired *k*-space lines, the first acquisition was used to compute the magnitude images. For each image, a threshold was set at 7% of the maximum intensity value within that image, and a mask was then generated from voxels with intensity values above the set threshold. Then, lines from central *k*-space that were acquired twice were used to compute a magnetic field map. The mask obtained from the magnitude image was used to select points in the magnetic field map for smoothing by least-squares fitting (using a singular value decomposition algorithm) of the masked points in the magnetic field map to a series of bivariate (x, y) polynomials up to the seventh order.

The smoothed field map was used to correct the distorted image in two steps. First, the central lines of raw *k*-space data for the image were shifted according to the phase values in the field map. Then the outer lines of *k*-space data were shifted half as much as the central lines. This is necessary because during acquisition, the edges of *k*-space are traversed twice as quickly as the center along the k_y direction, and the data acquired at the edges of *k*-space are distorted by magnetic field inhomogeneities only half as much as the data acquired at the center.

The distorted and corrected images generated by the MRTT sequence were compared to images obtained from a regular echo-planar scan using imaging parameters similar to those in the MRTT sequence, except for a shorter TE of 27.2 ms. The field map used for this correction was obtained by shifting the echo of the last pair of images in an echo-planar time series by 1 ms and 2 ms, and computing the phase difference between this pair of images. The correction algorithm was similar to the one used for the MRTT data, except here full *k*-space data were used (although they were still smoothed by least-squares fitting up to seventh-order bivariate polynomials), and the middle of *k*-space was shifted by the same amount as at the edges. With regular echo-planar trajectories, velocities are constant along the phase-encoding direction throughout all of *k*-space.

Monitoring B_0 Changes Arising From Tissue Displacement

To measure magnetic field changes due to susceptibility variations that arise from tissue displacement, experiments similar to those used to detect brain function (16) were used, and jaw movement and respiration were correlated with measured field changes. The subjects' behavior was cued with light. In the respiration experiments, the subjects exhaled when the light was turned off, and inhaled when the light was turned on. The cycle duration was 10 s, and each experiment consisted of 12 off/on cycles, with a 5-s off-period at the end. The same procedure and parameters were used for the jaw-movement experiments. The subject was instructed to keep his or her mouth closed when the light was off, to open when the light was on, and to hold it open until the light went off. Both image magnitude and magnetic field maps were calculated in all experiments.

The MRTT sequence was used with the following parameters: one 6-mm-thick slice located in the mid-sagittal plane was acquired with the readout direction parallel to B_0, FOV = 240 mm, image matrix = 96 × 96, 40 lines were collected twice to generate the field map, TR = 250 ms, and acquisition bandwidth = 166 kHz. This combination of parameters was chosen to establish a rate of six breaths per minute and provide 20 points per segment of the time course, so that the analysis software could provide a better estimate of field changes. A sagittal slice was used so that B_0 fluctuations would have a minimal impact on slice selection. Each respiration and jaw-movement experiment was repeated three times, and within each repetition 500 images were collected to generate the time series.

The fluctuations in magnetic field measured by the MRTT protocol, $\Delta B_{MRTT}(t)$, were modeled as originating from four sources: 1) changes caused by tissue displacement, $\Delta\chi_{tissue}(t)$ (the focus of the current experiments); 2) subject motion, whereby regions of tissue with different magnetic properties move in the FOV and cause signal changes in the time course that can show up as B_0 fluctuations, $\Delta B_{motion}(t)$; 3) linear field drifts over time, b_0; and 4) random noise, $\Delta B_{0,rand}(t)$. This can be represented by the equation:

$$\Delta B_{MRTT}(t) = \sum_{i=2}^{9} a_i \Delta\chi_{tissue}(t - i \cdot \mathrm{TR}) + \sum_{j=i}^{3} b_j \Delta B_{j,motion}(t) + b_0 \cdot t + \Delta B_{0,rand}(t). \quad [3]$$

To estimate a_i using Eq. [3], eight time-shifted versions of the stimulus waveform (i = 2,. . .,9) were used. These

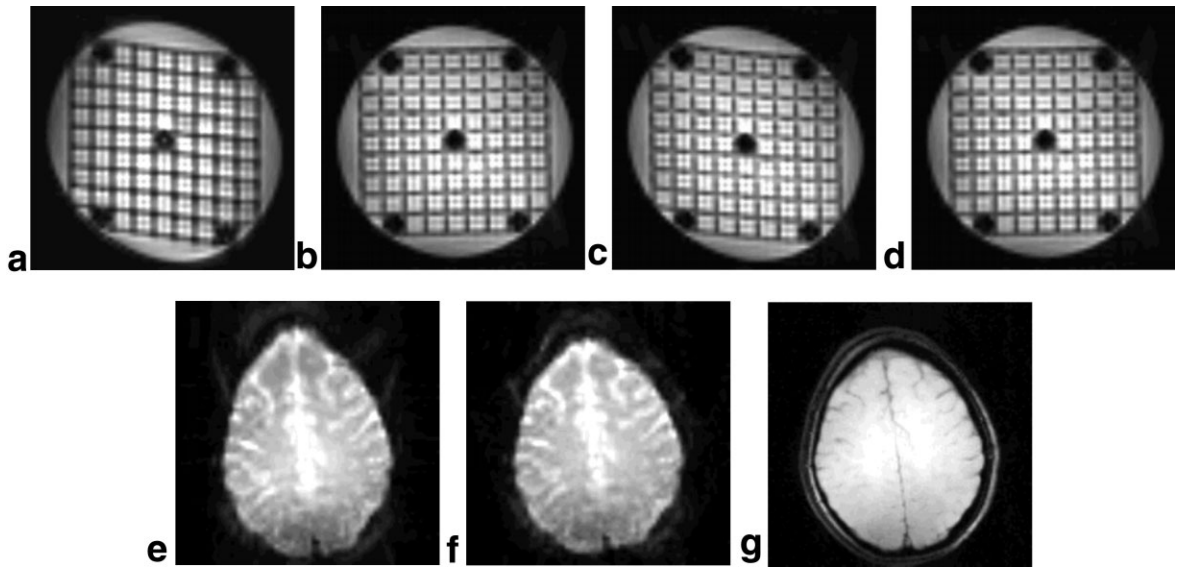

FIG. 2. (**a**) Uncorrected and (**b**) corrected in vitro MRTT images, compared with (**c**) uncorrected and (**d**) corrected echo-planar images resulting from a linear horizontal magnetic field gradient. Data used to compute image **a** were used for self-correction to generate image **b**. Image **c** was corrected using a map generated from the last two images in the time series, with TEs increased by 1 and 2 ms. (**e**) Uncorrected and (**f**) corrected MRTT, and (**g**) spin-warp in vivo images. Images **e** and **f** were treated in the same manner as images **a** and **b**.

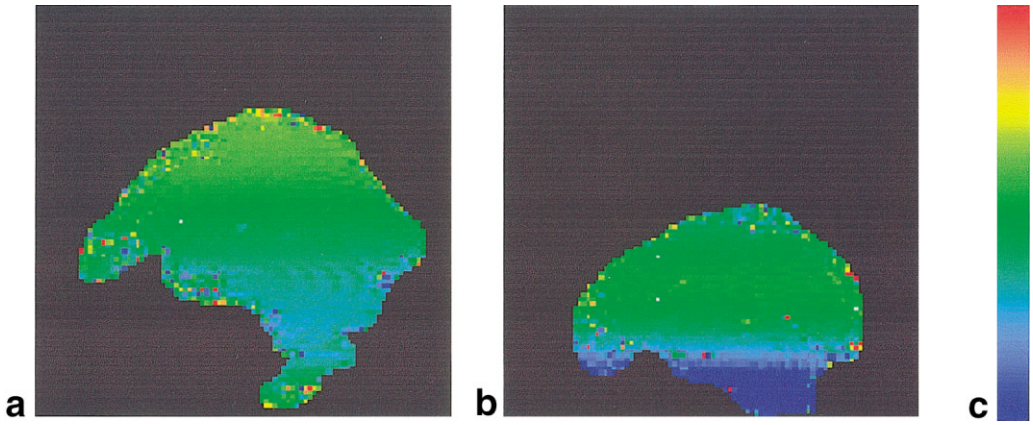

FIG. 3. Maps of magnetic field changes. **a:** Subject 1, second jaw-movement trial. **b:** Subject 2, second respiratory trial. **c:** Scale represents −0.25 to +0.25 ppm change.

corresponded to a response window of 0.5–2.5 s at the start of each segment of the time course, which allowed subjects 0.5 s to respond to the stimulus and another 2 s to complete the task. Magnitude images were used to estimate the time course of $\Delta B_{motion}(t)$, corresponding to the three in-plane motion parameters (translation along the two axes plus rotation), for each voxel time series. The motion parameters and time-shifted versions of the stimulus were input into Eq. [3], and values for a_i were obtained by using 3dDeconvolve (17). This program employs a least-squares method to fit the model to the measured ΔB_{MRTT} time series for each voxel. The coefficients that corresponded to the amplitudes of shifted versions of the stimulus time series (a_i) were summed and scaled to give results in parts per billion (ppb).

RESULTS

Geometric Corrections

Figure 2 shows both the purposely-distorted (a and c) and the corrected (b and d) images obtained using the MRTT protocol and EPI. Figure 2f (the corrected human data) corresponds to Fig. 2g (anatomical data) more closely than Fig. 2e (the uncorrected data). These images demonstrate the efficacy of the MRTT method in correcting magnetic field perturbations using only a fraction of *k*-space data. The time needed to acquire the image data plus the extra lines at the center of *k*-space for correction was <70 ms for the MRTT method, compared to 110 ms to collect a pair of images for the conventional gradient-recalled EPI method.

Monitoring B_0 Changes Arising From Tissue Displacement

Typical maps of magnetic field changes are shown in Fig. 3. Field changes were on the order of 25–50 ppb at the base of the brain (indicated by the horizontal light blue band in this region in both images). The standard deviations (SDs) of magnetic field changes over the entire brain were computed in all experiments for all subjects, and are presented in Table 1.

DISCUSSION

Weisskoff and Davis (6) used EPI-based magnetic field maps to perform geometric corrections to EPI data, and Nayak and Nishimura (7) successfully used magnetic field maps from a spiral scan to correct blurring in spiral data. Although the MRTT method is more prone to geometric distortions in lower-frequency image components due to the reduced velocity in the phase-encoding direction at the center of *k*-space, the magnetic field maps generated were shown to be of sufficient quality to perform geometric correction of distortions resulting from magnetic field perturbations. In fact, because the magnetic field maps are distorted to the same extent as the magnitude images, they are better suited for unwarping geometric distortions since the field perturbations register perfectly with the distortions they cause.

The magnetic field maps are computed from a reduced number of *k*-space lines. This does not pose a problem for geometric corrections because the $B_0(x, y)$ maps are further

Table 1
Standard Deviations of Magnetic Field Changes Over the Entire Brain

Subject	Respiration (trial no.)			Jaw movement (trial no.)		
	1	2	3	1	2	3
1	44.9	64.8	62.6	71.3	79.8	89.9
2	80.3	136.5	66.3	74.1	62.1	88.2
3	109.2	122.2	94.9	165.3	108.8	128.4
4	101.0	121.3	91.1	78.2	76.6	70.3
5	50.0	38.0	35.3	46.3	93.7	52.9

Magnetic field changes measured (in parts per billion) during respiration and jaw movement tasks.

smoothed to reduce the effects of phase noise. If higher-resolution field maps are required to determine magnetic field changes over smaller distances, more lines can be acquired. In this scenario, temporal resolution is traded for spatial resolution in the field maps, and can be optimized for a particular experiment. The reduced number of lines used to reconstruct the field map results in blurring along the phase-encoding direction, which is represented by the horizontal smearing in Fig. 3.

The magnetic field changes computed in these studies ranged from 35 to 165 ppb. The values for the jaw-movement experiments were larger than the 40–80 ppb reported by Birn et al. (11) for speech tasks. Similarly, the values measured in the respiration experiments were higher than those reported by Van de Moortele et al. (9) and Brosch et al. (10). Van de Moortele et al. (9) observed magnetic field changes of 0.7–5.4 Hz in axial slices (which at 7 T corresponds to magnetic field changes of 2–18 ppb), while the phase changes measured by Brosch et al. (10) showed fluctuations on the order of 10 ppb in mechanical simulations of human respiration at 1.5 T. The difference between the results presented here and those reported elsewhere may be due to the different regions from which data is used to compute B_0 fluctuations. Birn et al. (11) looked at variations from the inferior temporal lobe to the top of the brain, Brosch's results were obtained from a voxel at the center of the image, while Van de Moortele et al. (9) reported the average field variations from 10 axial slices with 10 mm separation. The values from this study represent the standard deviation of B_0 changes in a sagittal slice with a field of view of 240 mm, and include all regions from the top of the brain to the brain stem.

The use of magnetic field maps acquired on a per-image basis leads to better geometric correction of errors resulting from dynamic field perturbations. Recent studies by Ward et al. (18) and de Graaf et al. (19) showed the value of real-time correction of magnetic field perturbations. Ward et al. (18) demonstrated that real-time hardware compensation for linear magnetic field perturbations, which combined with prospective and retrospective motion correction improved image registration in nearly all cases beyond that obtained with retrospective motion correction alone. Improvement can be achieved by real-time updating of shim terms up to the second order, as shown by de Graaf et al. (19); however, they precalculated shim values for each slice and did not compensate for dynamic components. The method presented here has the potential to map and correct high-order dynamic field perturbations in real time by combining the methods developed in Refs. 18 and 19 into one technique. This will be useful for studies in which high-order magnetic field perturbations are generated and require correction in real time—for example, in fMRI studies utilizing speech tasks.

ACKNOWLEDGMENTS

The authors thank B. Ventura and K. Hyde for their assistance with the preparation of this manuscript.

REFERENCES

1. Jesmanowicz A, Hyde JS. Single-pass automatic 3D shimming. In: Proceedings of the 5th Annual Meeting of ISMRM, Vancouver, Canada, 1997. p 1983.
2. Jesmanowicz A, Roopchansingh V, Cox RW, Starewicz P, Punchard WFB, Hyde JS. Local ferroshims using office copier toner. In: Proceedings of the 9th Annual Meeting of ISMRM, Glasgow, Scotland, 2001. p 617.
3. Wilson JL, Jenkinson M, Jezzard P. Optimization of static field homogeneity in human brain using diamagnetic passive shims. Magn Reson Med 2002;48:906–914.
4. Jezzard P, Balaban RS. Correction for geometric distortion in echo planar images from B_0 field variations. Magn Reson Med 1995;34:65–73.
5. Roopchansingh V, Cox RW, Jesmanowicz A, Hyde JS. Magnetic field mapping in real time with a single RF pulse. In: Proceedings of the 10th Annual Meeting of ISMRM, Honolulu, 2002. p 2326.
6. Weisskoff RM, Davis TL. Correcting gross distortion on echo planar images. In: Proceedings of the 11th Annual Meeting of SMRM, Berlin, 1992. p 4515.
7. Nayak KS, Nishimura DG. Automatic field map generation and off-resonance correction for projection reconstruction imaging. Magn Reson Med 2000;43:151–154.
8. Raj D, Paley DP, Anderson AW, Kennan RP, Gore JC. A model for susceptibility artefacts from respiration in functional echo-planar magnetic resonance imaging. Phys Med Biol 2000;45:3809–3820.
9. Van de Moortele P-F, Pfeuffer J, Glover GH, Ugurbil K, Hu X. Respiration-induced B_0 fluctuations and their spatial distribution in the human brain at 7 Tesla. Magn Reson Med 2002;47:888–895.
10. Brosch JR, Talavage TM, Ulmer JL, Nyenhuis JA. Simulation of human respiration in fMRI with a mechanical model. IEEE Biomed Eng 2002; 49:700–707.
11. Birn RM, Bandettini PA, Cox RW, Jesmanowicz A, Shaker R. Magnetic field changes in the human brain due to swallowing or speaking. Magn Reson Med 1998;40:55–60.
12. Prammer MG, Haselgrove JC, Shinnar M, Leigh JS. A new approach to automatic shimming. J Magn Reson 1988;77:40–52.
13. Jesmanowicz A, Wong EC, Hyde JS. Phase correction of EPI using internal reference lines. In: Proceedings of the 12th Annual Meeting of SMRM, New York, 1993. p 1239.
14. Durand E, van de Moortele PF, Pachot-Clouard M, Le Bihan D. Artifact due to B_0 fluctuations in fMRI: correction using the *k*-space central line. Magn Reson Med 2001;48:198–201.
15. Wong EC, Bandettini PA, Hyde JS. Echo-planar imaging of the human brain using a three axis local gradient coil. In: Proceedings of the 11th Annual Meeting of SMRM, Berlin, 1992. p 105.
16. Bandettini P, Jesmanowicz A, Wong E, Hyde J. Processing strategies for time-course data sets in functional MRI of the human brain. Magn Reson Med 1993;30:161–173.
17. Ward BD. 2002. Deconvolution analysis of fMRI time series data. http://afni.nimh.nih.gov/AFNI/doc/3dDeconvolve.ps. Accessed 5 May 2003.
18. Ward HA, Riederer SJ, Jack CR. Real-time autoshimming for echo planar timecourse imaging. Magn Reson Med 2002;48:771–780.
19. de Graaf RA, Brown P, McIntyre S, Rothman DL, Nixon T. Dynamic shim updating (DSU) for multislice signal acquisition. Magn Reson Med 2003;49:409–416.